Complex dynamics of a spiral tip in the presence of an extrinsic local modulation

Seong-min Hwang, Won Gyu Choe, and Kyoung J. Lee*
National Creative Research Initiative Center for Neurodynamics and Department of Physics, Korea University, Seoul 136-701, Korea
(Received 3 April 2000; revised manuscript received 12 June 2000)

With a generic model excitable system, we have investigated the spatio-temporal dynamics of a spiral tip in the presence of an extrinsic *localized* periodic modulation. The tip of a modulated spiral does exhibit a variety of different trajectories depending on the strength and the frequency of the modulation. Its motion can be quasiperiodic on a 2-torus, quasiperiodic or mode locked on a 3-torus, or fully chaotic. Various bifurcations, including hard Hopf bifurcations and saddle-node bifurcations at strong resonances and period-doubling bifurcations of a mode-locked 3-torus, are revealed. In particular, the phenomenon of the period-doubling cascade of a resonant spiral tip trajectory is reported.

PACS number(s): 05.45.Ac, 82.40.Ck, 82.20.Wt, 82.40.Bj

I. INTRODUCTION

Rotating spiral waves are ubiquitous in nature and have long elicited the attention of researchers in a variety of different disciplines, including physics [1–4], chemistry [5–7], and biology [8–10]. Among others, of particular interest has been the spatiotemporal dynamics of a spiral tip (phase singularity) in excitable or oscillatory media [11–13]. While the spiral tip dynamics in homogeneous excitable media is now a well explored subject, the effects of extrinsic stimuli on the dynamics of a spiral tip are far less well understood, although they are of great importance.

From the standpoint of physics, the excitable or oscillatory system under external stimuli is a very interesting dynamical system that can result in a variety of rich and complex dynamics [14]. Moreover, understanding the effects of extrinsic stimuli to the natural system would have important implications in biology. For instance, a series of recent experimental and computational studies has discussed the interactions between pacemaking cells (i.e., external stimuli) and spiral waves on populations of dictyostelium discoideum. These studies have shown that the interaction can result in a particular ''prepattern,'' which in turn has a significant effect on the morphogenic development of the colony [10,15,16]. Also, there might be an important application in cardiology. It is very well known that spiral waves that form in heart tissue are closely related to various heart diseases [9]. These spiral waves, of course, can interact with the pacemaking heart cells. A recent study also indicated that the presence of abnormal cells in association with spiral waves in heart tissue can result in an abnormally fast heart beat, a deadly heart disease known as tachycardia [17]. Thus it is of interest to know the physics behind this interaction and the relevant biological implications [18].

In this article, we investigate the spatiotemporal dynamics of a spiral tip in the presence of a localized extrinsic periodic modulation (i.e., like a pacemaker periodically perturbing the system). The modulated tip undergoes very rich spatiotemporal dynamics, exhibiting phenomena of entrainment, mode locking, multistability, and chaos. Complex nonperiodic spiral tip trajectories were reported in past studies [19], but none of them have characterized the states and the bifurcations among them. Here, we provide clear analysis on various bifurcations among different tip trajectories, including the period-doubling cascade of a resonant tip trajectory. Our system differs from those of the earlier studies [14,20–22], which focus on the effects of spatially homogeneous modulations. In particular, our study is complementary to the recent work by Petrov *et al.* [14], who have studied resonant patterns in an oscillatory system with global periodic modulation in presence. To the best of our knowledge, a recent study by Rappel *et al.* [18] is the only report that addresses the effects of localized modulation. Their study focuses on the feasibility of using a discrete set of stimuli for controlling the undesirable wave instability that can occur in a set of equations modeling the dynamics of cardiac tissue.

Our model is described in Sec. II. The phenomenon of the period-doubling cascade of a resonant tip trajectory is presented in Sec. III, and various resonant states of a spiral tip trajectory forming a devil's staircase are discussed in Sec. IV. The size effect of a modulated region is discussed in Sec. V, and we conclude in Sec. VI.

II. MODEL

Our study is based on the following two species model:

$$\frac{\partial U}{\partial t} = F(U,V) + \nabla^2 U,$$

$$\frac{\partial V}{\partial t} = G(U,V) + \nabla^2 V + M(x_o, y_o, t; A, f_m),$$

where $F(U,V) = \epsilon^{-1} U(1-U)\{U-(V+b)/a\}$ and $G(U,V) = U - V$ are the kinetic functions and $M(x_0, y_0, t; A, f_m)$ models a localized periodic modulation. ϵ, a, and b are the system parameters. Except for the modulation term, the set of equations is a generic two-species reaction-diffusion model proposed earlier by Barkley [23]. The Barkley model is well known, not only for its efficiency in computation, but also for its faithful representation of many essential features of excitable systems.

*Author to whom correspondence should be addressed. Electronic address: kyoung@nld.korea.ac.kr

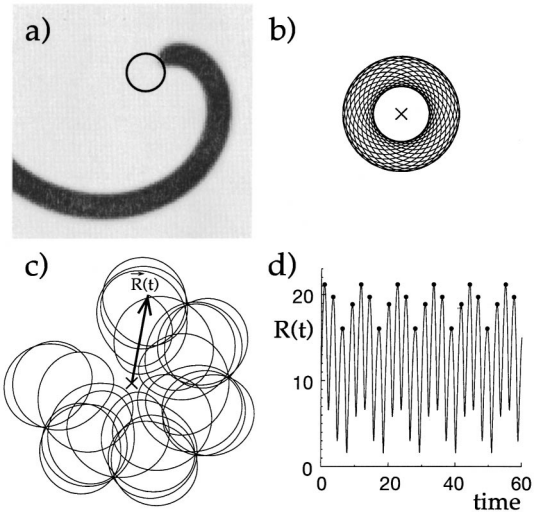

FIG. 1. The unmodulated (a) and the modulated [(b) and (c)] spiral tip trajectories in two dimensional space, and the time series of $R(t)$ corresponding to (c) in (d): $A=0$, $A=0.02$, and $A=0.1$ for (a), (b), and (c), respectively. The origin of the coordinate system was chosen as the site of modulation (marked with ''x'') and the spiral tip position $\vec{R}(t)$ is defined as the intersection of the two contours $U=0.5$ and $f(U,V)=0$. A snap shot of a simple spiral (U field, 96×96 domain) is shown in (a) together with its circular tip trajectory. The modulation frequency f_m is fixed at 0.37. While (b) and (c) are to scale, (a) is not to scale with (b) and (c).

The modulation term $M(x_o,y_o,t;A,f_m)$ is $A\sin(2\pi f_m t)$ within a small disk region (πr^2) located at (x_o,y_o) and 0 elsewhere. The disk is seeded near to a spiral core that is previously created and stabilized. The exact location of the disk is not important as long as it is within one pitch of the spiral core, since the perturbed spiral core will eventually be attracted and stabilized around the disk region. The dynamics of a spiral tip is investigated by varying the modulation frequency f_m and the amplitude A. The radius (r) of a modulated disk is fixed to be three except for those in Sec. V. The equations, all the variables, and the parameters are in dimensionless form.

The explicit Euler method is used for a 200×200 square grid with a no-flux boundary condition. The diffusion terms are evaluated by a finite difference nine-point formula after computing the reaction terms. The grid size and the (maximum) temporal step size that we employed are $\Delta x=0.16$ and $\Delta t=0.005$, respectively. These values guarantee the numerical stability [23]. Throughout this article, the distances are given in units of Δx and the time is given in units of $200\Delta t$.

III. PERIOD-DOUBLING BIFURCATIONS OF A SPIRAL TIP TRAJECTORY

Figure 1 illustrates three different types of orbits traced by a spiral tip, following a continuous increase in A [24]. Initially, a particular set of system parameters ($\epsilon=0.005$, $a=0.33$, $b=0.01$) is chosen to produce a simple spiral whose tip rotates steadily along a circle with a natural frequency $f_0=0.387\,931$ and radius $r_0=7.06$; see Fig. 1(a). Upon increasing A with f_m fixed, the simply periodic tip becomes unstable, moves gradually toward the modulation site, then stabilizes to execute a quasiperiodic motion following a hypocycloid — a compound orbit of two circular motions, where the primary circle (radius r_1) orbits the secondary circle (radius r_2) with frequency f_2 and spins about its center in the same direction with frequency f_1 [25]; see Fig. 1(b). The rotation frequency f_1 along the primary circle is locked to the modulation frequency f_m. For all hypocycloid orbits that we have examined, there is no evidence of mode locking as in the earlier studies on the meandering transition of unmodulated systems [12].

With a further increase in A, the hypocycloid orbit again becomes unstable to form a more complex compound orbit around the modulation site; see Fig. 1(c). The dynamics of this orbit can be better understood by investigating the time evolution of $R(t)$, the distance between the modulation site and the position of the tip, since it removes one rotational degree of freedom associated with the secondary circular orbit (r_2, f_2). The time series of R in Fig. 1(d) shows a composite oscillation with two different frequencies f_1 and f_3, where f_3 is a new frequency independent of f_1 and f_2. Thus we conclude that the complex compound orbit in Fig. 1(c) consists of three circular motions that lie on a 3-torus. The example shown in Fig. 1(c) is in particular a resonant state with $f_3:f_1=1:4$. The 1:4 resonance is clear in the time series of local maxima R_n, the return map of R_n, and the power spectrum of $R(t)$ in Fig. 2(a). The bifurcation from the quasiperiodic 2-torus [Fig. 1(b)] to the resonant state [Fig. 1(c)] is studied in greater detail and is found to be a saddle-node bifurcation immediately following a hard Hopf bifurcation to a 3-torus; the transition is hysteretic with a small but finite bistable region, as shown in the inset of Fig. 3. Although f_3 locks to f_1, f_2 does not lock to f_1 in a rational fraction; thus the resonant orbit is a particular one on a 3-torus with a partial mode locking.

Beyond the 1:4 resonant 3-torus state, we also find a period-doubling cascade. Somewhere between $A=0.415$ and $A=0.42$, the four resonant lines (in R_n), four points (in return map of R_n), and peaks [in the power spectrum of $R(t)$] in Fig. 2(a) all double to form a period-doubled 1:4 resonant state [Fig. 2(b)]. When A is further increased, the period-doubled 1:4 resonant state becomes unstable, doubling again to form the twice-doubled 1:4 resonant state as shown in Fig. 2(c). The subsequent cascade of period doubling ultimately leads to a chaotic state shown in Fig. 2(d). The bifurcation diagram shown in Fig. 3 summarizes the hysteretic transition and the period-doubling cascade.

IV. STRONG RESONANCE

Besides the subharmonic resonant states of 1:4 mode locking, other various resonant states also occur with a smaller value of f_m (i.e., further away from f_0) as shown in Fig. 4. In addition to the two primary resonances of 1:3 and 1:4, one secondary resonance $2:7=(1+1:3+4)$, three tertiary resonances $3:10=(1+2:3+7)$, $3:11=(2+1:7+4)$, $3:13=(1+2:4+9)$, and three fourth-order resonances $4:13=(1+3:3+10)$, $4:15=(3+1:11+4)$, $4:17=(1+3:4+13)$ are evident. The resonant states together form a devil's staircase as is seen in the well known case of a circle map. The question of the completeness of the staircase of Fig. 4 remains open due to the limits on our computational capability.

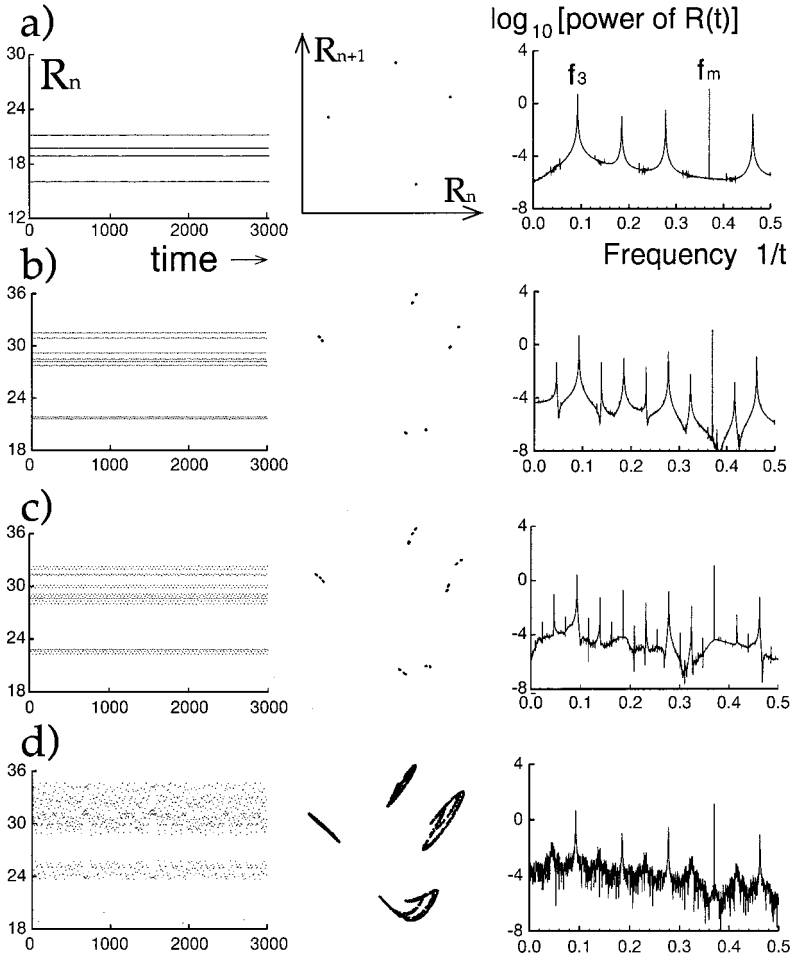

FIG. 2. Mode locking and period-doubling cascade of R_n with increasing value of A: (a) 1:4 resonance ($P4$), $A=0.1$, (b) period-doubled 1:4 resonance ($P8$), $A=0.5$, (c) twice-doubled 1:4 resonance ($P16$), $A=0.57$, and (d) chaotic state, $A=0.8$. The first, the second, and the third column, respectively, show time series of local maxima R_n of $R(t)$, return maps of R_n, and power spectra of $R(t)$. A fixed value of $f_m=0.37$ is used. A is given in $\log_{10}$ scale.

The bifurcations between resonant states and nearby nonresonant states are in general very complex. A detailed bifurcation sequence in the vicinity of the 1:3 resonant state in particular is shown in the inset of Fig. 4 and Fig. 5 shows some representative phase portraits along the bifurcation sequence. The dashed line in the inset corresponds to the stable quasiperiodic attractor on a 2-torus, the dotted line to the resonant attractor on a 3-torus, and the solid line to the nonresonant attractor on a 3-torus. In the return maps of Fig. 5, the quasiperiodic attractor on a 2-torus appears as a fixed point [the center dot in Figs. 5(a)–5(e)], the 1:3 resonant state as a period-3 cycle [Figs. 5(b) and 5(c)], and the nonresonant attractor on a 3-torus as a dotted loop [Figs. 5(e) and 5(f)]. For parameter values of A between the region 1 and 3, and between 4 and 5, the system is bistable.

The fixed point in Fig. 5(a) is stable and globally attracting below point 1. At point 1, a stable period-3 cycle is born via a saddle-node bifurcation [Fig. 5(b)]. Subsequently, the three elements in the period-3 cycle become unstable via a Hopf bifurcation at point 2, forming small element of the period-3 cycle [Fig. 5(c)]. The corresponding tip dynamics thus takes place on a 4-torus with an additional frequency f_4 with f_3 still mode locked with f_1. The attractor on 4-torus loses stability again at point 3 to return to the quasiperiodic state on a 2-torus [Fig. 5(d)]. At point 4, a pair of limit cycles (one stable and the other unstable) are created [Fig. 5(e)]. The unstable limit cycle shrinks toward the fixed point and disappears via subcritical Hopf bifurcation at point 5, beyond which only the nonresonant limit cycle is stable and globally attracting [Fig. 5(f)]. The transitions at points 4 and 5 are characteristic of a hard Hopf bifurcation.

Hysteretic transitions are also observed near the onset of other resonance states, but they can be quite different from that of 1:3 resonant state. For instance, the hysteretic transition at the left end of 1:4 resonance in Fig. 4 is caused by the competition between a resonant and a nonresonant attractor on a 3-torus. Below the point I, only a nonresonant limit cycle is stable and globally attracting. At point I, a periodic-4 cycle is created just outside the nonresonant limit cycle via a saddle-node bifurcation. At point II, the nonresonant limit cycle then disappears, colliding with another unstable limit cycle. Beyond the point II, the system is completely resonant.

V. SIZE EFFECT OF THE MODULATION REGION

Beside the modulation frequency f_m and the amplitude A, the size of the modulation region can also influence the dynamics of a spiral tip. However, we are only considering the effects of a small pacemaker that is about the size of a spiral core or smaller, and our numerical analysis shows that the size of modulation πr^2 simply has a similar role to that of A for the relevant physical situation. Figure 6 well confirms this point.

The mean values of R_n are plotted as a function of $\log_{10}$ (*modulation flux* $=\pi r^2 A$) in Fig. 6 for several different values of r. The data fit very well to a straight line and the onset of the Hopf bifurcation of a 2-torus leading to a 1:4 resonant

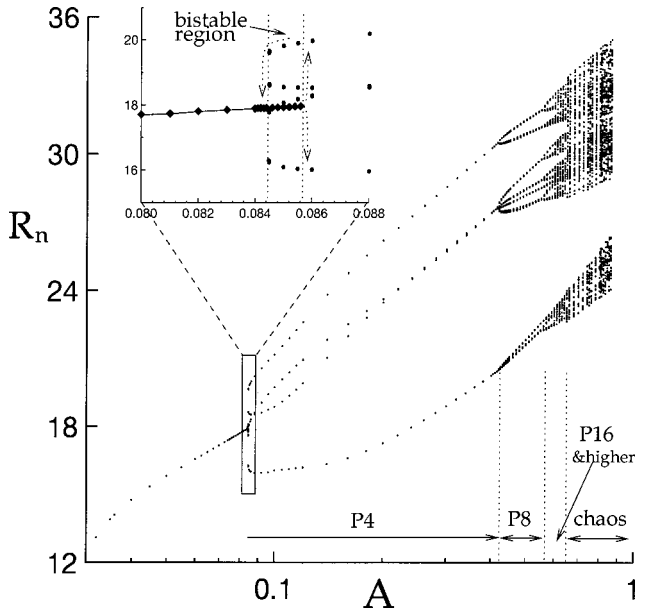

FIG. 3. Bifurcation diagram showing hysteretic transition to 1:4 resonance and period-doubling cascade. The inset figure shows the detail of the hysteresis at the onset of the 1:4 resonant state on a 3-torus. With increasing A (filled diamond) the transition occurs at about $A=0.0854$ and with decreasing A (filled circle) the transition back to a 2-torus occurs at a smaller value of about $A=0.0845$.

3-torus occurs at nearly the same value of *modulation flux* $\simeq 2.5$ and $R_n \simeq 18$ for all r but for $r=20$. This analysis indicates that the relevant bifurcation parameter controlling the dynamics of a spiral tip is *modulation flux* rather than f_m or A. Only when r becomes larger than 10 do the dynamics of a spiral tip become qualitatively different. Although exploring the bifurcation sequence of a spiral tip for large values of r can be an interesting issue, it is outside the scope of this article.

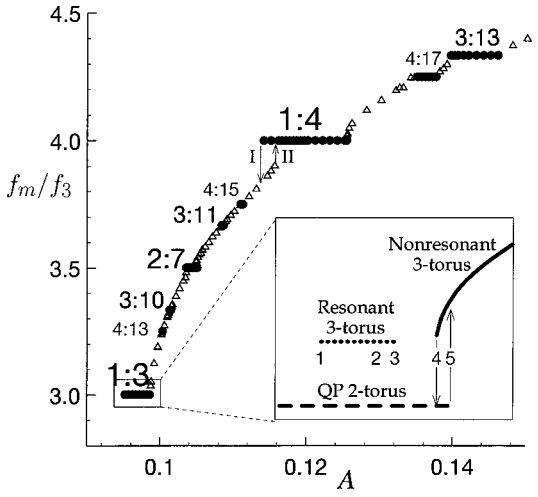

FIG. 4. Various resonant states shown in the f_3/f_m vs A plot. The resonant states with $f_m/f_3=3$, $3\frac{1}{4}$, $3\frac{1}{3}$, $3\frac{1}{2}$, $3\frac{2}{3}$, $3\frac{3}{4}$, 4, $4\frac{1}{4}$, and $4\frac{1}{3}$ are evident. The resonant (nonresonant) states are marked with filled circles (empty triangles). A fixed value of $f_m=0.355$ is used. The inset illustrates the complex bifurcation sequence showing the breakup of the 1:3 resonant state (discussed in the text).

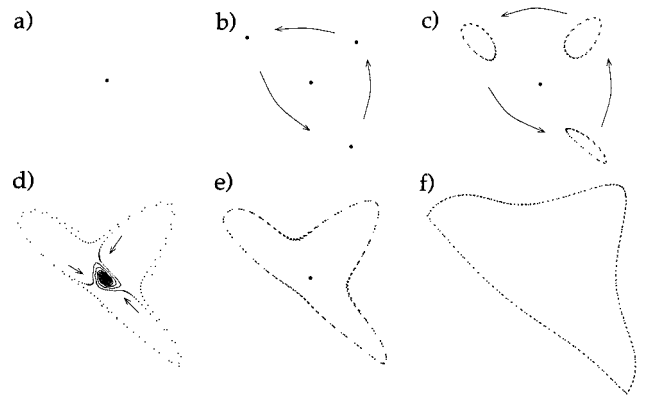

FIG. 5. Return maps of R_n along the bifurcation sequence shown in the inset of Fig. 4. With an increasing sequence of A, (a) quasiperiodic state on a 2-torus ($A=0.0920$ — before 1); (b) $f_3:f_1=1:3$ resonant state on a 3-torus ($A=0.0955$ — between 1 and 2); (c) $f_3:f_1=1:3$ resonant state on a 4-torus ($A=0.0980$ — between 2 and 3); (d) quasiperiodic state on a 2-torus ($A=0.0985$ — between 3 and 4); (e) quasiperiodic state on a 3-torus ($A=0.0986$ — between 4 and 5); and (f) quasiperiodic state on a 3-torus ($A=0.0995$ — after 5). Note that (b), (c), and (e) are bistable. In the map of (d), some transient flow is included to visualize the ''ghost'' loop. The arrows indicate the directions of flow.

VI. SUMMARY AND DISCUSSION

In summary, we have investigated the dynamics of a spiral tip under a localized extrinsic periodic modulation and found a wealth of complex attracting states: (1) for small values of A, the tip executes quasiperiodic motions on a 2-torus with no indication of mode locking; (2) for intermediate values of A, the tip either executes quasiperiodic motions with three incommensurate frequencies or partially mode-locked motions on a 3-torus; and (3) for large values of A, the tip motion ultimately becomes chaotic. Various bifurcations are also identified: (1) saddle-node bifurcations with hysteresis from quasiperiodic motions on a 2-torus leading to partially mode-locked states on a 3-torus; (2) the cas-

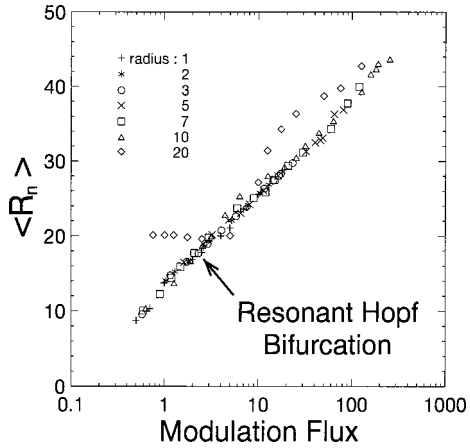

FIG. 6. Mean value of R_n vs *modulation flux* $=\pi r^2 A$ for different radii of the modulation disk. $\langle R_n \rangle$ is the arithmetic mean of R_n. The data fit well to a straight line $R_n \propto \log_{10}(\pi r^2 A)$. The 1:4 resonant Hopf bifurcation occurs at the marked position for all different radii except for *radius* $=20$. The *modulation flux* is given in $\log_{10}$ scale.

cade of period-doubling bifurcations leading to the chaotic motion; and (3) multistability between various attracting orbits.

In the future, resonant states for different modulation frequencies will be explored for a complete phase digram showing the structure of Arnold's tongues. We are also trying to build a low dimensional model that would capture the essential features that are revealed in this article. Finally, we suggest a relatively simple experiment to confirm our results. One can use the well known excitable Belousov-Zhabotinsky reaction with a light-sensitive catalyst such as the Ruthenium-bipyridil complex [20,14] in a continuously fed reactor; the localized sinusoidal modulation can be given by a tightly focused laser beam whose intensity is modulated in time.

ACKNOWLEDGMENTS

We are indebted to J. S. Lee for many helpful discussions. This work was supported by the Creative Research Initiatives of the Korean Ministry of Science and Technology.

[1] S. Jakubith, H. H. Rotermund, W. Engel, A. von Oertzen, and G. Ertl, Phys. Rev. Lett. **65**, 3013 (1990).
[2] E. Bodenschatz, J. de Bruyn, G. Ahlers, and D. S. Cannell, Phys. Rev. Lett. **67**, 3078 (1991).
[3] K. B. Migler and R. B. Meyer, Phys. Rev. Lett. **66**, 1485 (1991); K. B. Migler and R. B. Meyer, Physica D **71**, 412 (1994).
[4] P. Umbanhowar, F. Melo, and H. L. Swinney, Physica A **1**, 1 (1997).
[5] A. N. Zaikin and A. M. Zhabotinsky, Nature (London) **225**, 535 (1970).
[6] A. T. Winfree, Science **181**, 937 (1973).
[7] *Chemical Waves and Patterns*, edited by R. Kapral and K. Showalter (Kluwer, Dordrecht, 1995).
[8] L. Lechleiter, S. Girard, E. Peralta, and D. Clapham, Science **252**, 123 (1991).
[9] L. Glass, Phys. Today **49**(8), 40 (1996).
[10] K. J. Lee, E. C. Cox, and R. E. Goldstein, Phys. Rev. Lett. **76**, 1174 (1996).
[11] A. T. Winfree, Chaos **1**, 303 (1991).
[12] D. Barkley, Phys. Rev. Lett. **72**, 164 (1994).
[13] G. Li, Q. Ouyang, V. Petrov, and H. L. Swinney, Phys. Rev. Lett. **77**, 2105 (1996), and references therein.
[14] V. Petrov, Q. Ouyang, and H. L. Swinney, Nature (London) **388**, 655 (1997); A. Lin *et al.*, in *Pattern Formation in Continuous and Coupled Systems*, edited by M. Golubitsky, D. Luss, S. H. Strogatz (Springer, New York, 1999).
[15] K. J. Lee, Phys. Rev. Lett. **79**, 2907 (1997).
[16] E. Pálsson, K. J. Lee, R. E. Goldstein, J. Franke, R. H. Kessin, and E. C. Cox, Proc. Natl. Acad. Sci. U.S.A. **94**, 13 719 (1997).
[17] D. P. Zipes and J. Jalife, *Cardiac Electrophysiology: From Cell to Bedside* (W. B. Saunders, Philadelphia, 1995).
[18] W. Rappel, F. Fenton, and A. Karma, Phys. Rev. Lett. **83**, 456 (1999).
[19] W. Jahnke and A. Winfree, Int. J. Bifurcation Chaos Appl. Sci. Eng. **1**, 445 (1991).
[20] O. Steinbock, V. Zykov, and S. C. Müller, Nature (London) **366**, 322 (1993).
[21] A. P. Muñuzuri, M. Gómez-Gesteira, V. Pérez-Muñuzuri, V. I. Krinsky, and V. Pérez-Villar, Phys. Rev. E **50**, 4258 (1994).
[22] D. M. Goldschmidt, V. S. Zykov, and S. C. Müller, Phys. Rev. Lett. **80**, 5220 (1998).
[23] D. Barkley, M. Kness, and L. S. Tuckerman, Phys. Rev. A **42**, 2489 (1990); M. Dowle, R. M. Mantel, and D. Barkley, Int. J. Bifurcation Chaos Appl. Sci. Eng. **7**, 2529 (1997).
[24] We focus on the dynamics and bifurcations of a spiral tip by varying A for a few different fixed values of f_m that are close to but smaller than the natural frequency of the unmodulated spiral. When $f_m > f_0$, the spiral tip is gradually repelled away from the modulation site, as discussed in [15].
[25] The primary orbit is actually a slightly deformed circle (i.e., ellipse) as discussed in [12].